Atmos. Chem. Phys. Discuss., 13, 14797–14822, 2013
www.atmos-chem-phys-discuss.net/13/14797/2013/
doi:10.5194/acpd-13-14797-2013

Atmospheric Chemistry and Physics Discussions

Atmospheric waves as scaling, turbulent phenomena

J. Pinel and S. Lovejoy

Physics, McGill University, 3600 University St., Montreal, Quebec, Canada

Received: 15 February 2013 – Accepted: 17 May 2013 – Published: 5 June 2013

Correspondence to: S. Lovejoy (lovejoy@physics.mcgill.ca)

Published by Copernicus Publications on behalf of the European Geosciences Union.

Abstract

It is paradoxical that while atmospheric dynamics are highly nonlinear and turbulent that atmospheric waves are commonly modelled by linear or weakly nonlinear theories. We postulate that the laws governing atmospheric waves are on the contrary high Reynold's number (*Re*), emergent laws so that – in common with the emergent high *Re* turbulent laws – they are also constrained by scaling symmetries. We propose an effective turbulence – wave propagator which corresponds to a fractional and anisotropic extension of the classical wave equation propagator with dispersion relations similar to those of inertial gravity waves (and Kelvin waves) yet with an anomalous (fractional) order $H_{wav}/2$. Using geostationary IR radiances, we estimate the parameters finding that $H_{wav} \approx 0.17 \pm 0.04$ (the classical value = 2).

1 Introduction

The atmosphere is a highly turbulent system with the ratio of nonlinear to linear viscous terms – the Reynold's number – typically of the order $\approx 10^{12}$. At the same time, there is no doubt that atmospheric waves exist and play an important role in transferring energy and momentum. These empirical facts only become problematic when we consider the numerous apparently successful studies comparing data with linear (or weakly nonlinear) theory, commonly (for gravity waves) with the Taylor–Goldstein equations or with the linearized shallow water equations. For example, in the words of Nappo (2002) "Almost all of what we know about the nature of gravity waves is derived from the *linear theory*" (emphasis in the original).

Although one may easily get the impression that linear wave theories have been empirically confirmed, a closer look reveals that what has typically been scrutinized are the linear theory dispersion relations. Considering the example of gravity waves, we find that these have mostly been tested in the horizontal (and occasionally in the vertical) directions. Other predictions of the corresponding linear theory – "polarization

ACPD
13, 14797–14822, 2013

relations" – are invoked but are only used in a diagnostic mode so that they cannot be considered to have been convincingly validated (see e.g. Placke et al., 2013). Recently, linear gravity wave theory has been directly brought into question by data from dropsonde pairs. For example, such pairs have directly shown that certain terms neglected in the Taylor–Goldstein equations are typically much larger than the corresponding retained terms (Lovejoy and Schertzer, 2013). Also the pairs have clearly shown that the vertical structure of the atmosphere is composed of a fractal hierarchy of unstable layers through which linear gravity waves would not able to propagate (Lovejoy et al., 2008a).

The application of linear wave theories are generally justified in cases where the nonlinear terms are weak such as in theories of linear advection (e.g. Pielke, 2002) or more generally by the existence of large regions of laminar flow. However, since the 1980's – and largely thanks to the development of multifractal cascade models – there has been dramatic progress in understanding atmospheric intermittency (Schertzer and Lovejoy, 1987; Frisch, 1995). It is now clear that a prime characteristic of fully developed turbulence is that most of the important fluxes are concentrated in highly sparse (fractal) sets so that much of the flow appears relatively calm. The modern understanding is that by its very nature, turbulence is highly intermittent so that on any realization of a turbulent process, there will be violent regions in proximity to ones of relative calm. However, examination of the apparently calm regions shows that they also have embedded regions of high activity and as we zoom into smaller and smaller regions this strong heterogeneity continues in a scaling manner until we reach the dissipation scale (Tuck, 2010). This explains why aircraft measurements of the wind invariably find roughly $k^{-5/3}$ (i.e. turbulent) spectra even in apparently calm regions. Large scale regions of true laminar flow have yet to be documented by actual measurements. On the contrary, the multifractal, multiplicative cascade picture has been well verified even at large scales (e.g. Lovejoy and Schertzer, 2010). Therefore, it would be a mistake to separate these regions of high and low "turbulent intensities" and associate them with different mechanisms or to apply nonturbulent (linear) wave theories to regions of apparent calm.

ACPD
13, 14797–14822, 2013

In the last few years, (nonlinear) scaling theories of waves have become more compelling. This is because empirical evidence and theoretical arguments have amassed to the effect that atmospheric dynamics give rise to emergent high Reynolds number scaling laws with different horizontal and vertical exponents. This allows the horizontal scaling to accurately apply over huge ranges in scale, (see Lovejoy and Schertzer, 2010, 2013, for recent reviews). Although based on the classical laws of turbulence, they involve extensions to account for (multifractal) intermittency and anisotropy. Their success underlines the fundamental role of scale symmetries in constraining the high Re dynamics. All this motivates the question: are atmospheric waves also scaling turbulent phenomena? If this is the case, we may logically expect anomalous wave propagators that could readily have dispersion relations identical or nearly indistinguishable from their classical counterparts, while simultaneously having nontrivial consequences for the dynamics and for our understanding.

If dispersion relations from linear theory and those from strongly nonlinear theory can be very similar to each other, then how might one empirically distinguish them? The obvious way is to note that linear theory also predicts the entire space-time propagators relating the wave forcings and responses. A key characteristic of linear theories is that they involve integer powers of the (space and time) differential operators, and this strongly constrains the form of the propagators; below, we show how this allows us to test the theory by seeking possible anomalous propagator exponents. We investigate this using geostationary satellite infra red radiances.

The following paper attempts to show how scaling propagators with both turbulent and wavelike characteristics could arise while being consistent with both (anisotropic) turbulence theory and observations. However, let the reader be warned that while the turbulent part of the propagator – which was derived and empirically tested elsewhere (it is summarized here in an appendix) – is reasonably well grounded, in contrast, the wavelike part – the subject of this paper – is fairly speculative, it is perhaps little more than a proof of concept. On the theoretical side, the reason is that with only scaling symmetries to guide us, the possibilities are very broad while on the empirical

ACPD
13, 14797–14822, 2013

side, over the scaling range (120–5000 km in space and 3–100 h in time) the turbulent part of the spectrum is by far the dominant one accounting for an empirical range of spectral densities of a factor $\approx 10^5$ leaving the residual wavelike part to account for the remaining factor (which has a mean of 0.9 ± 0.5) in the dynamical spectral scaling range.

2 Fractional propagators and turbulence

In order to motivate our model, let's consider the classical wave equation for the wave I with forcing f:

$$\left(\nabla^2 - \frac{1}{V^2}\frac{\partial^2}{\partial t^2}\right) I(\underline{r}, t) = f(\underline{r}, t) \tag{1}$$

V is the wave velocity, $\underline{r}$ is the position vector and t the time variable.

As usual, we can solve Eq. (1) by taking Fourier transforms (denoted by tildas):

$$\tilde{I}(\underline{k}, \omega) = \tilde{g}(\underline{k}, \omega)\tilde{f}(\underline{k}, \omega); \quad \tilde{g}(\underline{k}, \omega) = \left(\omega^2/V^2 - |\underline{k}|^2\right)^{-1} \tag{2}$$

where $\underline{k}$ is the wavevector, ω the frequency and $\tilde{g}(\underline{k}, \omega)$ is the propagator. This propagator is symmetric with respect to an isotropic space-time scale transformation by factor λ^{-1}:

$$\tilde{g}\left(\lambda^{-1}\left(\underline{k}, \omega\right)\right) = \lambda^H \tilde{g}\left(\left(\underline{k}, \omega\right)\right); \quad H = 2 \tag{3}$$

However we anticipate that at high Re "effective propagators" may emerge constrained by the same overall scaling symmetry but with some other "anomalous" exponent $H \neq 2$. In this case we obtain fractional propagators corresponding to fractional gen-

ACPD
13, 14797–14822, 2013

eralizations of the wave equation:

$$\tilde{g}(\underline{k},\omega) = \left(\omega^2/V^2 - |\underline{k}|^2\right)^{H/2}; \quad \left(\nabla^2 - \frac{1}{V^2}\frac{\partial^2}{\partial t^2}\right)^{H/2} I(\underline{r},t) = f(\underline{r},t) \tag{4}$$

Although we will only require fractional propagators, if needed, we could define the fractional differential operator in Eq. (4) by the inverse Fourier Transform of $\tilde{g}(\underline{k},\omega)^{-1}$ (or see e.g. Miller and Ross, 1993 for fractional differential equations). If we seek the real space solution of Eq. (1) or (4), we can use the fact that Fourier space products (Eq. 2) correspond to real space convolutions ("*") hence the solutions to Eqs. (1) and (4) are: $I(\underline{r},t) = g(\underline{r},t) * f(\underline{r},t)$ so that the propagator links the forcing (f) to the response (I).

In order to estimate the $g(\underline{r},t)$ we can appeal to the method of stationary phase (e.g. Bleistein and Handelsman, 1986) which ensures us that the dominant contribution to $g(\underline{r},t)$ is due to the wavenumber-frequency region over which $\tilde{g}(\underline{k},\omega)$ is singular, this singularity defines the dispersion relation and accounts for its origin and significance. For both the classical Eq. (1) and the nonclassical Eq. (4), we find the dispersion relation:

$$\omega = \pm V \left|\underline{k}\right| \tag{5}$$

which is therefore of fundamental importance, a fact which is true for any $H > 0$, not only for positive even integer values of H.

Before attempting to estimate propagators of real data, we must take into account the fact that atmospheric waves occur in the presence of turbulence. Indeed the spectrum is so strongly dominated by a "turbulent background" that it must first be removed before evidence of any wavelike propagator can be observed. This is paradoxical since the wavelike part implies the existence of a singular set over a surface in (k_x, k_y, ω) space and should be easy to detect (actually, the topology need not be so simple, see Sect. 5). However, the singularity is of sufficiently low order and spectral estimates

ACPD
13, 14797–14822, 2013

are sufficiently noisy that in practice the singular set is hard to observe. Indeed it is much easier to study 2-D subspaces obtained by integrating out one of the spectral coordinates (which also reduces the "noise"), although if H is small enough (and this is indeed the case here, see below) this can integrate out the singularities. Indeed, one of the main techniques for empirically investigating atmospheric waves (Wheeler and Kiladis, 1999; Hendon and Wheeler, 2008; Dias et al., 2012) integrated over k_y space to yield a (k_x, ω) 2-D spectrum while also using an ad hoc averaging technique for removing the turbulent contribution.

Following Wheeler and Kiladis (1999), we also use infra red data (but at hourly not daily resolution), we use instead a theoretically motivated turbulent spectrum to search for evidence of anomalous wave propagators. To understand this, recall the classical Kolmogorov law of three dimensional isotropic turbulence:

$$\Delta I\left(\underline{\Delta r}\right) = \varphi \left|\underline{\Delta r}\right|^{H}; \quad \varphi = \varepsilon^{1/3}; \quad H = 1/3 \tag{6}$$

where I is a component of the wind, ΔI is a fluctuation, $\underline{\Delta r}$ is a vector displacement, ε is the turbulent energy flux and the equality is understood in a statistical sense. In Fourier space this becomes:

$$\tilde{I}\left(\underline{k}\right) = \tilde{g}_{\text{tur}}\left(\underline{k}\right)\tilde{\varphi}\left(\underline{k}\right); \quad \tilde{g}_{\text{tur}}\left(\underline{k}\right) = \left|\underline{k}\right|^{-H} \tag{7}$$

comparing this with Eq. (2), we see that $\tilde{\varphi}\left(\underline{k}\right)$ is the forcing and $\tilde{g}_{\text{tur}}\left(\underline{k}\right)$ is the spatial part of a (fractional order) propagator (a Green's function). Now recall that for real I, that $\tilde{I}\left(\underline{k}\right) = \tilde{I}^{*}\left(-\underline{k}\right)$, if in addition we assume statistical translational invariance ("statistical homogeneity"), then we may define the spectral densities P_I, P_φ, by:

$$\left\langle \tilde{I}\left(\underline{k}\right)\tilde{I}\left(\underline{k}'\right)\right\rangle = \delta\left(\underline{k}+\underline{k}'\right)P_I\left(\underline{k}\right); \quad \left\langle \tilde{\varphi}\left(\underline{k}\right)\tilde{\varphi}\left(\underline{k}'\right)\right\rangle = \delta\left(\underline{k}+\underline{k}'\right)P_\varphi\left(\underline{k}\right) \tag{8}$$

so that $P_I\left(\underline{k}\right) \propto \langle|\tilde{I}|^2\rangle$, $P_\varphi\left(\underline{k}\right) \propto \langle|\tilde{\varphi}|^2\rangle$ where "$\langle\rangle$" denotes ensemble averaging and "δ" is the Dirac δ function.

ACPD
13, 14797–14822, 2013

To obtain the classical Kolmogorov–Obhukhov $k^{-5/3}$ law we use:

$$P_\varphi(\underline{k}) = P_0 \left|\underline{k}\right|^{-s_\varphi} \; ; \quad s_\varphi = d - K(2) \tag{9}$$

where P_0 is a dimensional constant, d is the dimension of space and $K(2)$ is the second order intermittency correction exponent. This yields:

$$P_l(\underline{k}) = P_\varphi(\underline{k})|\tilde{g}_{\text{tur}}|^2 = P_0 \left|\underline{k}\right|^{-s_\varphi - 2H} = P_0 k^{-s_\varphi - 2H} \; ; \quad k = \left|\underline{k}\right| \tag{10}$$

The angle integrated ("isotropic") spectral density $E(k)$ is then given by integrating P over shells in Fourier space. Ignoring constant factors (2π in $d = 2$, 4π in $d = 3$), we obtain the (intermittency corrected) isotropic Kolmogorov law:

$$E(k) \approx P_l(k)\, k^{d-1} = k^{-\beta}; \quad \beta = 1 + 2H - K(2) \tag{11}$$

(since $H = 1/3$, we see that the nonintermittent $K(2) = 0$ case does indeed have exponent $\beta = 5/3$).

A basic consequence of wide range spatial scaling of atmospheric fields (in particular the wind) is that the spectrum and spectral density of the turbulent fluctuations in horizontal wavenumber – frequency (k_x, k_y, ω) space follow the straightforward space-time extension of Eq. (6):

$$\tilde{I}(\underline{k}, \omega) = \tilde{g}_{\text{tur}}(\underline{k}, \omega)\tilde{\varphi}(\underline{k}, \omega); \quad P_l(\underline{k}, \omega) = \left|\tilde{g}_{\text{tur}}(\underline{k}, \omega)\right|^2 P_\varphi(\underline{k}, \omega) \tag{12}$$

where $P_l(\underline{k}, \omega)$, $P_\varphi(\underline{k}, \omega)$ are space-time spectral densities, $\tilde{g}_{\text{tur}}(\underline{k}, \omega)$ is the turbulent propagator. To obtain the form of $\tilde{g}_{\text{tur}}(\underline{k}, \omega)$, we follow (Lovejoy and Schertzer, 2010; Pinel et al., 2013) outlined in appendix A (see Eq. A13) to obtain the dimensionless propagator:

$$\tilde{g}_{\text{tur}}(\underline{k}, \omega) = \left(i\omega' + \left\|\underline{k}\right\|\right)^{-H_{\text{tur}}} \tag{13}$$

ACPD
13, 14797–14822, 2013

where:

$$\omega' = \left(\omega + \underline{k}\cdot\underline{\mu}\right)\sigma^{-1}; \quad \sigma = \left(1 - \left(\mu_x^2 + a^2\mu_y^2\right)\right)^{1/2}; \quad \left\|\underline{k}\right\| = \left(k_x^2 + a^2 k_y^2\right)^{1/2} \tag{14}$$

where k_x, k_y and ω have been nondimensionalized as discussed in appendix A, using the size of the Earth and the turbulent velocity V_w and $\underline{\mu} = (\mu_x, \mu_y)$ is the mean dimensionless horizontal advection vector. $\left\|\underline{k}\right\|$ is the (horizontal) spatial (Fourier) scale function and a is the north-south/east-west aspect ratio; when $a = 1$, we obtain $\left\|\underline{k}\right\| = \left|\underline{k}\right|$ (note that if needed, more complex spatial scale functions may be used : these scale functions replace the vector norms in the isotropic theories). The transformation $\omega \rightarrow \omega'$ combines the effects of a mean advection by velocity $\underline{\mu}$ and the statistical variability of the advection wind about its mean (via σ). Note that (a) the factor i in Eq. (13) is necessary so that the propagator respects causality, and (b) overall $\tilde{g}_{\text{tur}}$ respects the same isotropic scaling symmetry as the wave propagator, Eq. (3) but with exponent H_{tur}.

3 Fractional propagators and waves

With the exception of the weak singularities associated with waves, the turbulence dominates the spectral density, the $P_I(\underline{k}, \omega)$ given in Eq. (12) with the propagator Eq. (13) already gives a good approximation to the empirical spectral density. This may be seen in Fig. 1 using MTSAT data (described below) which shows the 1-D spectral densities $E(k_x)$, $E(k_y)$, $E(\omega)$ obtained by successively integrating out various pairs of variables from $P_I(k_x, k_y, \omega)$, (see Pinel et al., 2013). This log-log linearity on this figure directly shows that the spectra are scaling and near perfect superposition of the 1-D spectra demonstrates that the scaling exponents are essentially identical so that (in conformity with the conclusions of appendix A and the form Eq. 13) the radiance field structure functions are symmetric with respect to isotropic scale changes $(\Delta x, \Delta y, \Delta t) \rightarrow \lambda^{-1}(\Delta x, \Delta y, \Delta t)$ or equivalently, $(k_x, k_y, \omega) \rightarrow \lambda(k_x, k_y, \omega)$. This

ACPD
13, 14797–14822, 2013

turbulence part corresponds to the "background" spectrum obtained by Wheeler and Kiladis (1999); any wave behaviour is to be found in deviations from this.

A simple model that takes into account waves while respecting both the space-time scaling and the turbulent forcing and background is obtained by including a factor $\tilde{g}_{\text{wav}}$ in the overall propagator. To be "wave-like", $\tilde{g}_{\text{wav}}$ must be causal, unlocalized in space-time and must also be chosen so that the overall scaling symmetry of the system (Eq. 3) is respected by the overall propagator $\tilde{g}_I\left(\underline{k},\omega\right)$. Following Wheeler and Kiladis (1999) who factored the spectral density into a "red noise" turbulent background and a wave part and inspired by Eqs. (2) and (13), we can use the form:

$$\tilde{I}\left(\underline{k},\omega\right) = \tilde{g}_I\left(\underline{k},\omega\right)\tilde{\varphi}\left(\underline{k},\omega\right) \;; \quad \tilde{g}_I\left(\underline{k},\omega\right) = \tilde{g}_{\text{tur}}\left(\underline{k},\omega\right)\tilde{g}_{\text{wav}}\left(\underline{k},\omega\right) \tag{15}$$

with $\tilde{g}_{\text{tur}}$ given by Eq. (13) and $\tilde{g}_{\text{wav}}$ given by:

$$\tilde{g}_{\text{wav}}\left(\underline{k},\omega\right) = \left(\omega'^2/v_{\text{wav}}^2 - \left\|\underline{k}\right\|^2\right)^{-H_{\text{wav}}/2} \tag{16}$$

This is a generalization of Eq. (2) to account for spatial anisotropy (with $\left|\underline{k}\right| \rightarrow \left\|\underline{k}\right\|$). The replacement $\omega \rightarrow \omega + \underline{k}\cdot\underline{\mu}$ is the classical advection transformation (see e.g. Nappo, 2002); as in the turbulent propagator, we have included the extra factor σ to take into account the statistical variation of the advection velocity (see Eq. 14). Finally, the parameter v_{wav} is the phase speed nondimensionalized by the turbulent velocity V_w (Eq. 13). Note that the overall propagator $\tilde{g}_I$ satisfies the scaling symmetry Eq. (3) with $H = H_{\text{tur}} + H_{\text{wav}}$. Due to $\tilde{g}_{\text{wav}}$, the overall propagator $\tilde{g}_I$ yields the dispersion relation:

$$\omega = -\underline{k}\cdot\underline{\mu} \pm \sigma v_{\text{wav}}\left\|\underline{k}\right\| \tag{17}$$

With respect to the "background" advection ($\underline{\mu}$), σv_{wav} is the effective wave speed which takes into account the mean wave speed (v_{max}) and the statistical variability via σ. By taking appropriate scale functions $\left\|\underline{k}\right\|$ one can obtain dispersion relations close to gravity and other waves (see Lovejoy et al., 2008b). Although the dispersion relation

ACPD
13, 14797–14822, 2013

is independent of the propagator exponent H_{wav}; the exponent does determine the (power law) rate of decay of the forcing so that the value of H_{wav} will affect the transport of momentum and energy.

Of more relevance here are Kelvin waves which are the low Coriolis parameter/high "effective thickness" limit of the inertial gravity (Poincaré) wave dispersion relations often invoked at these space-time scales. First, for only one spatial (zonal) dimension, we may note that Kelvin waves are a special case of Eq. (17) with $\left\|\underline{k}\right\| = k_x$. Considering the full horizontal plane, Kelvin waves are "channelled"; they only propagate in the zonal direction. To obtain some channeling while maintaining the same overall scaling symmetry, we could replace the spatial (Fourier) scale function $\left\|\underline{k}\right\| = \left(k_x^2 + a^2 k_y^2\right)^{1/2}$ by $\left\|\underline{k}\right\| = \left(k_x^2 - a^2 k_y^2\right)^{1/2}$ which only allows meridional propagation for small scale (high wavenumber) structures. For example, when $\underline{\mu} = 0$, large structures with $k_x < \omega/(\sigma v_{wav})$ cannot propagate in the meridional direction, they are "channelled".

Finally, combining Eqs. (13), (15) and (16), we obtain the turbulent – wave spectral density:

$$P_l(\underline{k},\omega) = P_\varphi(\underline{k},\omega)\left|\tilde{g}_{tur}\right|^2\left|\tilde{g}_{wav}\right|^2$$

$$P_l(\underline{k},\omega) = P_\varphi(\underline{k},\omega)\left(\omega'^2 + \left\|\underline{k}\right\|^2\right)^{-H_{tur}}\left(\omega'^2/v_{wav}^2 - \left\|\underline{k}\right\|^2\right)^{-H_{wav}};$$

$$P_\varphi(\underline{k},\omega) = P_0\left(\omega'^2 + \left\|\underline{k}\right\|^2\right)^{-s_\varphi/2} \quad (18)$$

In Eq. (18), we have followed the assumption in the isotropic case (Eq. 10) that the forcing of the flux has the same scale symmetries as $\left|\tilde{g}_{tur}\right|^2$; from Eq. (A13) we see that $s_\varphi = d - K(2)$ is the spectral exponent of the flux and, P_0 a dimensional constant determined by the climatological (low frequency) average forcing.

ACPD
13, 14797–14822, 2013

4 Data analysis

We follow Wheeler and Kiladis (1999) and Hendon and Wheeler (2008) but estimate the turbulent background using regressions to estimate the parameters of $\tilde{g}_I$ (i.e. of $\tilde{g}_{\text{tur}}$ and $\tilde{g}_{\text{wav}}$). The data set was comprised of 1386 images (∼ two months of data, September and October 2007) of radiances measured by the first "thermal" infrared channel (10.3–11.3 µm, particularly sensitive to temperature near the top of clouds) of the geostationary satellite MTSAT over south-west Pacific at resolutions 30 km and 1 h over latitudes 40° S–30° N and longitudes 80° E–200° E. We separated the sample into five 277 h (∼ 12 day) blocks, calculating for each block, the spectral density of fluctuations of the field with respect to the mean image (we used a standard Hann window to reduce spectral leakage). Note that as opposed to Wheeler and Kiladis (1999) who averaged their data in order to estimate the turbulent contribution to the signal, we rather averaged our data to obtain a better statistical estimate of the ensemble spectrum, the regression to the theoretical form provides the smooth "background".

To see how a purely turbulent spectrum already provides a good approximation, we performed a multivariate regression on the empirical MTSAT spectral density and theoretical form (Eq. 18) with $H_{\text{wav}} = 0$. Figure 1 shows the 1-D spectra obtained by integrating the 3- D density over the complementary coordinates using $s_\varphi = 2.88 \pm 0.01$ and $H_{\text{tur}} = H = 0.26 \pm 0.05$. The fit is good over the range of scales 120–5000 km in space and 3–100 h in time (except for small diurnal contributions at 12 and 24 h), it is especially good if we numerically take into account finite sample size effects at the large and small scales (the curvature in the black line in Fig. 1). The excellent superposition confirms the scale symmetry of the type Eq. (3): $P_I\left(\lambda^{-1}(\underline{k},\omega)\right) = \lambda^{s_I} P_I(\underline{k},\omega)$ with $s_I = s_\varphi + 2H = 3.4 \pm 0.1$ (Eq. 18).

We now consider the three 2-D spectra, obtained by successively integrating the 3-D spectral density over k_x, k_y and ω. The fit is sufficiently good that we can use the above regression with $H_{\text{wav}} = 0$ to estimate all the turbulent parameters. However for the 1-D spectra to have fixed exponents, when fitting the wave part we must use the constraint

ACPD
13, 14797–14822, 2013

$H = H_{tur} + H_{wav}$ so that the 1-D spectral slopes are not affected. In this way we find an optimum relative weighting for the turbulence and wave contributions. Figure 2a, b, d show these for three different values of H_{wav}. As before, the purely turbulent ($H_{wav} = 0$) case gives a good fit with mean deviations ±11 % in $\mathrm{Log}_{10}P(k,\omega)$ in the three 2-D spaces (excluding the diurnal spikes and the origin) which is small considering that the 2-D space signal $P(k,\omega)$ varies over ∼ four orders of magnitude. The orientations of the contours of $P(k_x,\omega)$, $P(k_y,\omega)$ is a consequence of the non zero mean zonal velocity $\overline{v_x} \sim -12 \pm 4\,\mathrm{km\,h^{-1}}$ and smaller mean meridional velocity $\overline{v_y} \sim 4 \pm 3\,\mathrm{km\,h^{-1}}$, the wave part is the residual: $|\tilde{g}_{wav}|^2 \propto P_l \left(\omega'^2 + \left\|\underline{k}\right\|^2\right)^{s_\varphi/2+H_{tur}}$, see Eq. (18). Although this is noisy, the value $H_{wav} \approx 0.17 \pm 0.04$ (so that $H_{tur} = H - H_{wav} = 0.09 \pm 0.06$; $H = 0.26 \pm 0.05$ is fixed) gives the best overall fit and nondimensional wave speed $v_{wav} = 1.0 \pm 0.8$. Recall that the case $v_{wav} = 1$ means the wave speed is equal to that of the turbulent wind. Note that even though $H_{wav} > H_{tur}$, the turbulence still dominate the overall spectrum: due to the factor P_φ (Eq. 18) one should compare $s_\varphi + 2H_{tur} \sim 3.06$ with $2H_{wav} \sim 0.34$.

In order to isolate the wave contribution to the spectrum, Wheeler and Kiladis (1999) removed a "turbulent background" (estimated with an ad hoc averaging technique) from their (k_x,ω) 2-D spectrum and tried to identify maxima in the residual with linear theory dispersion relations. Following them, we removed (by dividing) from the empirical 3-D spectral density the "turbulent background" estimated from the fit of Eq. (18) with $H_{wav} = 0$ (i.e. the purely turbulent spectral density from which we obtained Fig. 2a). The residual from which wave behaviour is to be identified (and which is to be described by the wave part of Eq. 18) is presented in Fig. 3 for the (k_x,ω) 2-D space with $\omega > 0$ (i.e. after integrating over k_y). We observe a region of maxima (Fig. 3 in grey) for $k_x > 0$ which is similar to the residual obtained by Wheeler and Kiladis (1999) although for larger wavenumbers and frequencies. Also shown in Fig. 3 is the theoretical dispersion relation for Kelvin waves which was obtained by Wheeler and Kiladis (1999) (compare with their Fig. 3 for the equivalent depth $h = 12$ m).

ACPD
13, 14797–14822, 2013

A key point about Kelvin waves and Fig. 3 is that they are asymmetrical in the zonal direction (k_x). In contrast, the simple form of $\tilde{g}_{wav}$ used in Eq. (18) involves a Fourier space scale function $\|\underline{k}\| = \left(k_x^2 + a^2 k_y^2\right)^{1/2}$ which is symmetrical in $\underline{k}$ and which involves, in the (k_x, ω) space, maxima lines (coming from the singularities) for $k_x > 0$ as well as for $k_x < 0$, which is incompatible with Fig. 3 (grey region). However, the only constraints on the form of $\tilde{g}_{wav}$ are that it must respect causality, that g is real, (hence $\tilde{g}\left(\underline{k}, \omega\right) = \tilde{g} * \left(-\underline{k}, -\omega\right)$) and that the overall scaling symmetry (Eq. 3) is respected. We can therefore modify the form of $\tilde{g}_{wav}$ so that it is no longer invariant under $k_x \rightarrow -k_x$ For example, the following form is adequate:

$$\tilde{g}_{wav}(\underline{k}, \omega) = \left\{ i \left(\omega' / v_{wav} + \|\underline{k}\| \text{sign}(\underline{k} \cdot \underline{\mu}) \right) \right\}^{-H_{wav}}; \quad \|\underline{k}\| = \left(k_x^2 + a^2 k_y^2\right)^{1/2} \tag{19}$$

Replacing $\tilde{g}_{wav}$ in Eq. (18) by Eq. (19) preserves the quality of the fit of the total (turbulent-wave) spectral density, (see the 2-D subspaces in Fig. 2c) and gives a spectra $P_{wave}(k_x, \omega)$ close to the data, including a maxima line which is close to the maxima in the residual presented in Fig. 3. With this asymmetrical propagator, we find that the only parameters that change significantly are $v_{wav} = 1.4 \pm 0.8$; $H_{wav} = 0.08 \pm 0.04$ (so that $H_{tur} = H - H_{wav} = 0.18 \pm 0.06$).

5 Refined singularity analysis

The above analysis is paradoxical since our hypothesis is that there is a singular set in (k_x, k_y, ω) space yet analysis of the 1-D and 2-D sections showed no direct evidence of singular behaviour. This is consistent with the finding that $0 < H_{wav} < 1$ implying that the singularities are integrated out in the lower dimensional sections. In order to display potential singularities, we are therefore forced to study the full 3-D density $P(k_x, k_y, \omega)$ recognizing that most of the variation is due to the turbulent part and that the wave part – being only weakly singular – is expected to manifest itself in maxima, perhaps

ACPD
13, 14797–14822, 2013

with surface-like topology (line-like in 2-D sections). If one considers 2-D sections of $P(k_x, k_y, \omega)$ – for instance for ω fixed – and using a landscape analogy, these maxima would be either isolated peaks or crests of mountain ranges (including saddle points in such crests). To detect these peaks or crests, we implemented an ad hoc singularity detection algorithm that "scans" parallel to the axes to estimate maxima successively in the k_x, k_y directions (for ω fixed). In principle considering the maxima in a single direction is adequate, but in practice the singular surface has parts that are roughly parallel to a given axis; the resulting ambiguity can be resolved by determining maxima in two orthogonal directions.

The results are shown in Fig. 4, where we compare such an analysis with the theoretical behaviour (with $\tilde{g}_{\text{wav}}$ from Eq. 19) for constant ω sections. A drawback of the method is that it does not distinguish maxima due to the turbulent contribution and from the (presumed) wave contribution and in the empirical case, the separation is not always evident. In the figure, the two have been distinguished by the color of the lines. We see that although far from perfect, the semi ellipses indicating the theoretical singularity (dispersion relation) are close to the empirical ones. Given that we used a straightforward generalization of the classical wave equation with only one new parameter v_{wav} (two if we include $H_{\text{wav}} = 0.08$, but this doesn't affect the singular surface) and given that the wave part of the overall propagator Eq. (16) as well as the postulated multiplicative decomposition (Eq. 15) are not much more than the simplest analytical hypotheses, the results are quite encouraging, yet they indicate some of the difficulties.

6 Conclusions

The atmosphere is highly nonlinear yet displays both turbulent and wavelike behaviour over huge ranges of space-time scales. Theories explaining the turbulent aspects assume that the dynamics are strongly nonlinear and scaling, in contrast, the corresponding wave theories are generally linear or weakly nonlinear. We proposed that the paradox can be explained by noting that although linear theory predicts propagators, only

ACPD
13, 14797–14822, 2013

the relations implied by the singular part of the latter – the dispersion relations – have been tested to any extent. However, linear theories invariably involve integer differential operators and corresponding integer ordered propagators so we may test these theories by examining the propagators – or at least their squared moduli which are amenable to empirical spectral determination.

The mathematical structure of the turbulent laws that link the observables to driving turbulent fluxes (such as energy fluxes) use scaling (turbulent) propagators which are very similar to that of wave equations except that the latter are singular. To account for both waves and turbulence, the actual propagators need only respect scale symmetries and can be modelled as products of turbulent-like and wave-like (space-time localized and unlocalized) propagators with both involving anomalous exponents. The wave propagator we used involves the mean horizontal turbulent wind and energy flux as well as a mean background wave advection velocity, obtained as an (anisotropic, fractional) generalization of the classical wave equation (which is approximately satisfied by inertial gravity waves and Kelvin waves). Using two months of MTSAT hourly geostationary IR radiances, using a simple form for the wave propagator, we found that the best fit involved an anomalous wave scaling exponent $H_{wav} \approx 0.17 \pm 0.04$; for comparison, the classical wave equation has the integer value $H_{wav} = 2$. Since the propagator determines the rate at which the forcing decays, such an anomalous exponent will affect the transport of energy and momentum and thus has implications for the dynamics.

Investigating the wave structure, we followed Wheeler and Kiladis (1999), dividing our empirical spectral density by a theoretically estimated "turbulent background"; the maxima in the residual are to be identified with wave dispersion relations. Since there are very few theoretical constraints on the form of the wave propagator, we chose a simple ansatz that is compatible with the observations.

This paper is simply an early attempt to understand waves in highly turbulent media using scaling symmetries as constraints. On the one hand, these symmetries are so broad that they provide only limited guidance, on the other hand, the turbulent part –

ACPD
13, 14797–14822, 2013

with no wave contribution at all – explains almost all of the observed dynamical spectral scaling range of factor $\approx 10^5$ leaving only a small residual (a factor which has a mean of 0.9 ± 0.5) for the wavelike part. The empirical situation would certainly be improved if data from other fields covering wide scale ranges in the full (x, y, z, t) space could be found, but at present the (x, y, t) geostationary radiances are apparently the best available. Therefore, this paper should be seen more as a proof of concept than as providing definitive results. The main conclusion is thus that strongly turbulent atmospheric dynamics are a priori compatible with the observed waves, that to understand them, that one needn't invoke the existence of large laminar regimes nor linear theories.

Appendix

The space-time turbulent spectrum

The 23/9D model of spatial turbulence Schertzer and Lovejoy (1985a, b) involves wide range scaling in the horizontal and vertical directions but with different scaling exponents; the horizontal being dominated by energy fluxes, and the vertical by buoyancy variance fluxes. Since the infra red radiances are essentially (x, y, t) (horizontal-time) fields we needn't explicitly consider the vertical, however we do need to extend the model to space-time. In this appendix, we summarize the arguments developed in Lovejoy et al. (2008b), Lovejoy and Schertzer (2010, 2013) and in Pinel et al. (2013).

The first step is to rewrite the isotropic Eq. (6) in a more general anistropic scaling manner by replacing the vector norm by a space-time scale function $[[\underline{\Delta R}]]$:

$$\Delta I\left(\underline{\Delta R}\right) = \varphi_{[[\underline{\Delta R}]]}\left[[\underline{\Delta R}]\right]^{H} \tag{A1}$$

where we have used the subscript $[[\underline{\Delta R}]]$ to emphasize that the flux is at resolution $[[\underline{\Delta R}]]$. The space-time scale function is symmetric with respect to generalized scale

ACPD
13, 14797–14822, 2013

changes T_λ:

$$[[T_\lambda \underline{\Delta R}]] = \lambda^{-1} [[\underline{\Delta R}]] \; ; \quad T_\lambda = \lambda^{-G} \tag{A2}$$

where G is the generator of the scale changing operator T_λ. Ignoring for the moment advection, and taking I as a horizontal velocity component then the canonical (simplest) nondimensional scale function compatible with the Kolmogorov law is:

$$[[\underline{\Delta R}]] = L_w \left\{ \left(\frac{\Delta x}{L_w} \right)^2 + \left(\frac{\Delta y}{L_w / a} \right)^2 + \left(\frac{\Delta t}{\tau_w} \right)^{2/H_t} \right\}^{1/2} \tag{A3}$$

where $H_t = (1/3)/(1/2) = 2/3$ and L_w, τ_w are the outer scales of the scaling in space and in time and a is a north-south/east-west aspect ratio. The outer scales are linked by the overall average energy flux $\varepsilon : \tau_w = \varepsilon^{-1/3} L_w^{2/3}$ (τ_w is the lifetime/"eddy-turn-over time" of structures size L_w). Successively substituting $\underline{\Delta R} = (\Delta x, 0, 0)$, $\underline{\Delta R} = (0, \Delta y, 0)$, $\underline{\Delta R} = (0, 0, \Delta t)$ into Eq. (A3) and the latter into Eq. (A1), yields the Kolmogorov law in the horizontal directions (e.g. $\Delta v = \varepsilon^{1/3} \Delta x^{1/3}$) and time, the Lagrangian law ($\Delta v = \varepsilon^{1/2} \Delta t^{1/2}$).

The next step is to consider the scale function corresponding to a constant advection in the horizontal $\underline{v} = (v_x, v_y)$. Due to Gallilean invariance, (i.e. under $x \rightarrow x - v_x \Delta t \; ; \; y \rightarrow y - v_y \Delta t \; ; \; \Delta t \rightarrow \Delta t$) we obtain:

$$[[\underline{\Delta R}]] = L_w \left\{ \left(\frac{\Delta x - v_x \Delta t}{L_w} \right)^2 + \left(\frac{\Delta y - v_y \Delta t}{L_w / a} \right)^2 + \left(\frac{\Delta t}{\tau_w} \right)^{2/H_t} \right\}^{1/2} \tag{A4}$$

Since there is no scale separation, $\underline{v}$ is a turbulent velocity, so that over a given region, it will be dominated by the advection due to the largest eddies. For the same reasons,

ACPD
13, 14797–14822, 2013

the link between L_w and τ_w is via a turbulent velocity ($V_w = L_w/\tau_w$), a consequence of which is that the pure temporal development (Lagrangian) term may be neglected.

Denoting the scale function obtained by averaging over the ensemble of different advection velocities as the "effective" scale function; it is obtained by averaging

$$[[\underline{\Delta R}]] = \left(\frac{\Delta x - v_x \Delta t}{L_w}\right)^2 + \left(\frac{\Delta y - v_y \Delta t}{L_w/a}\right)^2 \quad \text{(A5)}$$

over the turbulence (this argument is not completely rigorous since due to the intermittency, averaging over other powers of $[[\underline{\Delta R}]]$ will give somewhat different parameters). Turbulence will have two effects on Eq. (A5): the mean advection by $\underline{v}$, and the effect of turbulent variability. The overall result (for more details, see Pinel and Lovejoy, 2013) is:

$$\left\langle \Delta I \left(\underline{\Delta R}\right)^2 \right\rangle = \left\langle \varphi^2_{[[\underline{\Delta R}]]_{\text{eff}}} \right\rangle [[\underline{\Delta R}]]^{2H}_{\text{eff}} \quad \text{(A6)}$$

where the effective scale function is given by:

$$[[\underline{\Delta R}]]_{\text{eff}} = \left(\underline{\Delta R}^T \underline{\underline{B}} \Delta R\right)^{1/2}; \quad \underline{\underline{B}} = \begin{pmatrix} 1 & 0 & -\mu_x \\ 0 & a^2 & -a^2\mu_y \\ -\mu_x & -a^2\mu_y & 1 \end{pmatrix} \quad \text{(A7)}$$

where we have used the nondimensional variables:

$$\underline{\Delta R} \rightarrow \underline{\Delta R} = \left(\frac{\Delta x}{L_w}, \frac{\Delta y}{L_w}, \frac{\Delta t}{\tau_w}\right); \quad \underline{\mu} = (\mu_x, \mu_y) = \left(\overline{v_x}, \overline{v_y}\right)/V_w \quad \text{(A8)}$$

where $\underline{\overline{v}} = (\overline{v_x}, \overline{v_y})$ is the overall mean advection over the region considered and $V_w = (\overline{v_x^2} + a^2\overline{v_y^2})$ is the large-scale turbulent velocity at planetary scale.

ACPD
13, 14797–14822, 2013

The intermittency corrections come from the scaling of the flux φ:

$$\left\langle \varphi^2_{[[\underline{\Delta R}]]_{\text{eff}}} \right\rangle \approx \left[\left[\underline{\Delta R}\right]\right]^{-K(2)}_{\text{eff}} \tag{A9}$$

so that overall:

$$\left\langle \Delta I \left(\underline{\Delta R}\right)^2 \right\rangle \approx \left[\left[\underline{\Delta R}\right]\right]^{\xi(2)}_{\text{eff}} \tag{A10}$$

The structure function exponent $\xi(2) = 2H - K(2)$ thus takes into account the scaling exponent H as well as the intermittency correction.

To obtain the corresponding spectral density $P_I(\underline{k}, \omega)$ (and hence, $\tilde{g}_{\text{tur}}(\underline{k}, \omega)$), we follow the development presented by Lovejoy and Schertzer (2010) (see also Pinel et al., 2013) and use the general relation between structure functions and spectra: $\left\langle \left| \Delta I(\underline{\Delta R}) \right|^2 \right\rangle = 2 \int_{-\infty}^{\infty} d\underline{K} \left(1 - e^{i\underline{K}\cdot\underline{\Delta R}}\right) P_I(\underline{K})$; with nondimensionalized wavevector $\underline{K} = \left(L_w k_x, L_w k_y, \tau_w \omega\right)$ so that the effective real space scale function (that takes into account the averaging over an ensemble of advection velocities) defines an effective Fourier space scale function:

$$\left[\left[\underline{K}\right]\right]_{\text{eff}} = \left(\underline{K}^T \underline{\underline{B}}^{-1} \underline{K}\right)^{-1/2}; \quad \underline{\underline{B}}^{-1} = \begin{pmatrix} 1 - a^2\mu_y & \mu_x\mu_y & \mu_x \\ \mu_x\mu_y & \left(1 - \mu_x^2\right)/a^2 & \mu_y \\ \mu_x & \mu_y & 1 \end{pmatrix} \tag{A11}$$

using:

$$\omega' = \left(\omega + \underline{k}\cdot\underline{\mu}\right)\sigma^{-1}; \quad \sigma = \left(1 - \left(\mu_x^2 + a^2\mu_y^2\right)\right)^{1/2} \tag{A12}$$

this can be simplified to: $\left[\left[\underline{K}\right]\right]_{\text{eff}} = \left(\omega'^2 + \left\|\underline{k}\right\|^2\right)^{1/2}$ where $\left\|\underline{k}\right\|^2 = k_x^2 + \left(k_y/a\right)^2$ is the (horizontal) spatial (Fourier) scale function. The transformation $\omega \rightarrow \omega'$ combines the

ACPD
13, 14797–14822, 2013

effects of a mean advection by velocity $\underline{\mu}$ and the statistical variability of the advection wind about its mean is accounted for by $\underline{\sigma}$.

With this scale function, we have the nondimensional spectra:

$$P_I\left(\underline{K}\right) = |\tilde{g}_{\text{tur}}|^2 P_\varphi\left(\underline{K}\right); \quad |\tilde{g}_{\text{tur}}|^2 \approx \left[\left[\underline{K}\right]\right]_{\text{eff}}^{-2H}; \quad P_\varphi\left(\underline{K}\right) = \left[\left[\underline{K}\right]\right]_{\text{eff}}^{-d+K(2)} \tag{A13}$$

(with $d = 3$ for horizontal space-time).

References

Bleistein, N. and Handelsman, R. A.: Asymptotic Expansions of Integrals, Mineola, Dover, 1986.

Dias, J., Tulich, S. N., and Kiladis, G. N.: : An object based approach to assessing tropical convection organization, J. Atmos. Sci., 69, 2488–2504, 2012.

Frisch, U.: Turbulence: The Legacy of A. N. Kolmogorov, Cambridge University Press, Cambridge, 296 pp., 1995.

Hendon, H. H. and Wheeler, M.: Some space-time spectral analyses of tropical convection and planetary waves, J. Atmos. Sciences, 65, 2936–2948, 2008.

Lovejoy, S. and Schertzer, D.: Towards a new synthesis for atmospheric dynamics: space-time cascades, Atmos. Res., 96, 1–52, doi:10.1016/j.atmosres.2010.1001.1004, 2010.

Lovejoy, S. and Schertzer, D.: The Weather and Climate: Emergent Laws and Multifractal Cascades, Cambridge University Press, Cambridge, 2013.

Lovejoy, S., Tuck, A. F., Hovde, S. J., and Schertzer, D.: Do stable atmospheric layers exist?, Geophys. Res. Lett., 35, L01802, doi:10.1029/2007GL032122, 2008a.

Lovejoy, S., Schertzer, D., Lilley, M., Strawbridge, K. B., and Radkevitch, A.: Scaling turbulent atmospheric stratification, Part I: Turbulence and waves, Q. J. Roy. Meteor. Soc., 134, 316–335, doi:10.1002/qj.1201, 2008b.

Matsuno, T.: Quasi-geostrophic motions in the equatorial area, J. Meteorol. Soc. Jpn., 44, 25–43, 1966.

Miller, K. S. and Ross, B.: An Introductiona to the Fractional Calculus and Fractional Differential Equations, Wiley-Interscience, New-York, 1993.

Nappo, C. J.: An Introduction to Gravity Waves, Academic Press, Amsterdam, 276 pp., 2002.

ACPD
13, 14797–14822, 2013

Pielke, R. A.: Mesoscale meteorological modeling, 2nd edn., Academic Press, San Diego, CA, 676 pp., 2002.
Pinel, J., Lovejoy, S., and Schertzer, D.: The horizontal space-time scaling and cascade structure of the atmosphere and satellite radiances, Atmos. Res., submitted, 2013.
Placke, M., Hoffmann, P., Gerding, M., Becker, E., and Rapp, M.: Testing linear gravity wave theory with simultaneous wind and temperature data from the mesosphere, J. Atmos. Sol.-Terr. Phy., 93, 57–69, 2013.
Schertzer, D. and Lovejoy, S.: The dimension and intermittency of atmospheric dynamics, in: Turbulent Shear Flow 4, edited by: Launder, B., Springer-Verlag, Berlin, 7–33, 1985a.
Schertzer, D. and Lovejoy, S.: Generalised scale invariance in turbulent phenomena, Physicochem. Hydrodyn., 6, 623–635, 1985b.
Schertzer, D. and Lovejoy, S.: Physical modeling and analysis of rain and clouds by anisotropic scaling multiplicative porcesses, J. Geophys. Res., 92, 9692–9714, 1987.
Tuck, A. F.: From molecules to meteorology via turbulent scale invariance, Q. J. Roy. Meteor. Soc., 136, 1125–1144, 2010.
Wheeler, M. and Kiladis, G. N.: Convectively coupled equatorial waves: analysis of clouds and temperature in the wavenumber-frequency domain, J. Atmos. Sci., 56, 374–399, 1999.

ACPD
13, 14797–14822, 2013

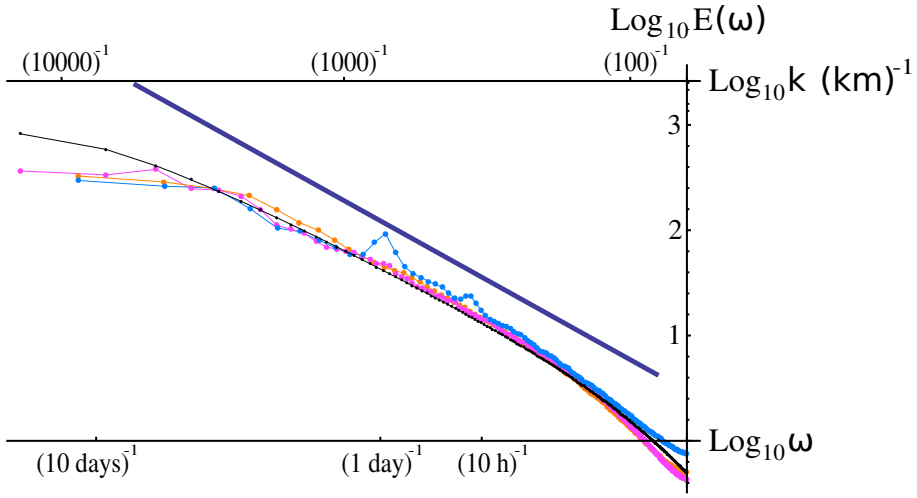

Fig. 1. 1-D spectra from MTSAT data; blue: temporal; orange: meridional; purple: zonal and a multivariate regression curved due to the finite empirical domain; black, using $H_{wav} = 0$, $V_w = 41 \pm 3\,km\,h^{-1}$; $\tau_w = L_e/V_w \approx 20 \pm 1$ days; $a \approx 1.2 \pm 0.1$; $s_l \approx 3.4 \pm 0.1$; $P_0 = 2.8 \pm 0.2\,^{\circ}C^2\,km^2\,h$; $\mu_x \approx -0.3 \pm 0.1$; ($\overline{v_x} \approx -12 \pm 4\,km\,h^{-1}$); $\mu_y \approx 0.10 \pm 0.08$; ($\overline{v_y} \approx 4 \pm 3\,km\,h^{-1}$), $\sigma = 0.95 \pm 0.03$.

ACPD
13, 14797–14822, 2013

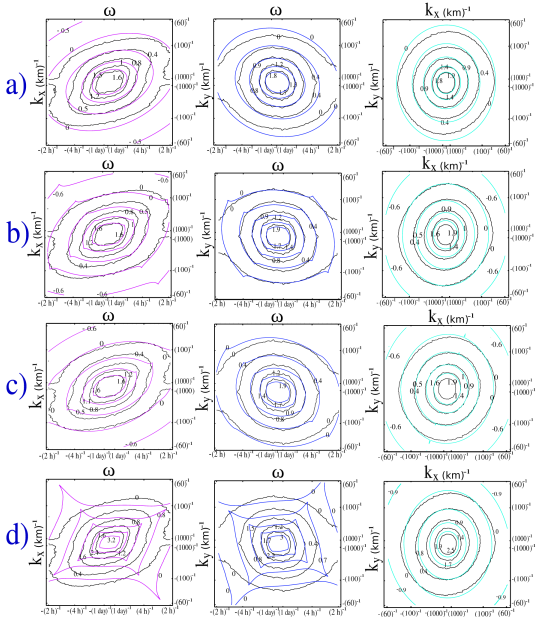

Fig. 2. Comparison of 2-D spectral densities from MTSAT data (in black) and a multivariate regression from theoretical $P_I(\underline{k}, \omega)$ given by Eq. (18) (in color). The 2-D subspaces (left to right) are (ω, k_x), (ω, k_y) and (k_x, k_y). The ranges are ω from $(2\,\mathrm{h})^{-1}$ to $(277\,\mathrm{h})^{-1}$; k_x from $(60\,\mathrm{km})^{-1}$ to $(\approx 13\,000\,\mathrm{km})^{-1}$ and k_y from $(60\,\mathrm{km})^{-1}$ to $(\approx 8000\,\mathrm{km})^{-1}$. **(a)** with imposed $H_{\mathrm{wav}} = 0$ which corresponds to the purely turbulent case. (with $H_{\mathrm{tur}} = H - H_{\mathrm{wav}}$, $H = 0.26 \pm 0.05$, $s_\varphi = 2.88 \pm 0.01$). The other parameters are $V_w = 41 \pm 3\,\mathrm{km\,h^{-1}}$; $\tau_w = L_e/V_w \approx 20 \pm 1$ days; $a \approx 1.2 \pm 0.1$; $s_I \approx 3.4 \pm 0.1$; $P_0 = 2.8 \pm 0.2\,^\circ\mathrm{C}^2\,\mathrm{km}^2\,\mathrm{h}$; $\mu_x \approx -0.3 \pm 0.1$; ($\overline{v_x} \approx -12 \pm 4\,\mathrm{km\,h^{-1}}$); $\mu_y \approx 0.10 \pm 0.08$; ($\overline{v_y} \approx 4 \pm 3\,\mathrm{km\,h^{-1}}$) hence, $\sigma = 0.95 \pm 0.03$ and nondimensional wave speed $v_{\mathrm{wav}} = 1.0 \pm 0.8$. **(b)** $H_{\mathrm{wav}} = 0.17 \pm 0.04$ (best fit value). **(c)** Fit from Eq. (18) with $\tilde{g}_{\mathrm{wav}}$ from Eq. (19). $H_{\mathrm{wav}} = 0.08 \pm 0.04$ and $v_{\mathrm{wav}} = 1.4 \pm 0.8$. **(d)** Same parameters as **(a)**, but with imposed $H_{\mathrm{wav}} = 1$.

ACPD
13, 14797–14822, 2013

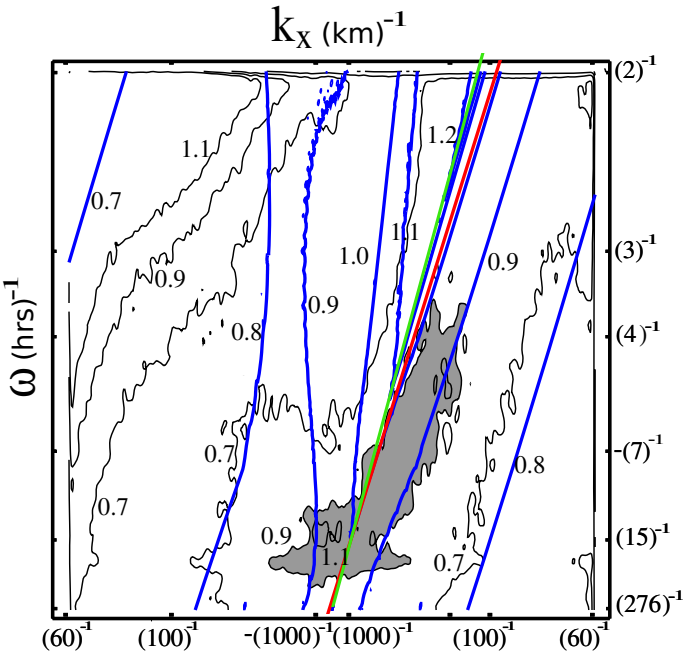

Fig. 3. Contour plot in the 2-D (k_x, ω) space (i.e. $P(k_x, k_y, \omega)$ is integrated over k_y) Black lines: the empirical spectral density divided by the "turbulent background" (i.e. the fit of Eq. (18) with imposed $H_{wav} = 0$); region of maxima relevant to Kelvin waves indicated (in grey). Blue lines: $|\tilde{g}_{wav}|^2 = \left|\omega'/v_{wav} + \left|\left|\underline{k}\right|\right| \mathrm{sign}(\underline{k} \cdot \underline{\mu})\right|^{-2H_{wav}}$ with parameters $H_{wav} = 0.08 \pm 0.04$; $v_{wav} = 1.4 \pm 0.8$, integrated over k_y, (the maximal line is indicated in green). In red: the dispersion relation for Kelvin waves (corresponding to $h = 12$ m) in Fig. 3 of Wheeler and Kiladis (1999).

ACPD
13, 14797–14822, 2013

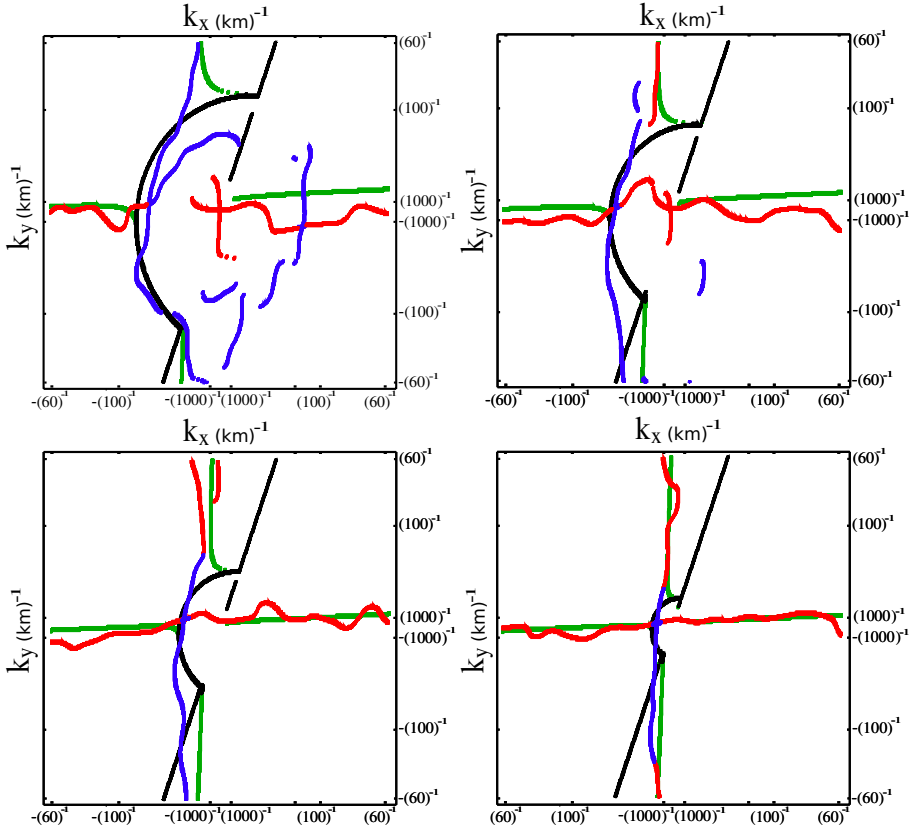

Fig. 4. Left to right, top to bottom, four (k_x, k_y) sections of $P(k_x, k_y, \omega)$ for $\omega = 2, 3, 5, 10\,\mathrm{h}^{-1}$, the origin is in the centre. The black line is the theoretical singularity (dispersion) curve $(|\tilde{g}_{\mathrm{wav}}|^2$ with $\tilde{g}_{\mathrm{wav}}$ from Eq. 19); the blue, the empirically estimated curve using the ad hoc algorithm and the green and red show maxima but presumed to originate in the turbulence "background" (they are very close to the axes).

ACPD
13, 14797–14822, 2013

Atmospheric waves as scaling, turbulent phenomena

J. Pinel and S. Lovejoy